POLYCRYSTALLINE GaN LAYER ON M-PLANE SAPPHIRE SUBSTRATE FOR METAL-SEMICONDUCTOR-METAL PHOTODETECTOR

AZHARUL ARIFF BIN KAMARULZAMAN

UNIVERSITI SAINS MALAYSIA

2017

POLYCRYSTALLINE GaN LAYER ON M-PLANE SAPPHIRE SUBSTRATE FOR METAL-SEMICONDUCTOR-METAL PHOTODETECTOR

by

AZHARUL ARIFF BIN KAMARULZAMAN

Thesis submitted in fulfillment of the requirement
for the degree of
Doctor of Philisophy

December 2017

ACKNOWLEDGEMENT

Alhamdulillah, finally this work is done. Let this thesis show what can be done by creating, innovating and going against the norm when a researcher is faced with limited facility.

This work would not be completed without MyPhD scholarship bestowed by Malaysian Ministry of Higher Education, and also the various sponsorships from research grants and Institute of Post Graduate Studies (USM). Special credit should be given for Dr. Norzaini Zainal, who took the time and effort to closely guide my work as a PhD. candidate. To Prof. Zainuriah Hassan, thank you for your advice when the time was rough. To my colleagues; Esmed, Ikram, Ezzah, Waheeda, and Alvin, thank you for inspiring me through your work. Technical assistance from the staff of Institute of Nano Optoelectronics Research and Technology (INOR) is greatly appreciated.

To my mother, thank you for your patience and prayers. For my father, you have always set good examples for us to follow. With the experience and knowledge that was gained here, I hope that I am one step closer to become you. Finally, I would like to express my gratitude to *'Waifu'*, who have been supporting me physically and emotionally during the final parts of this work. Let's grow old together.

TABLE OF CONTENTS

ACKNOWLEDGEMENT ii

TABLE OF CONTENTS iii

LIST OF TABLES vii

LIST OF FIGURES ix

LIST OF SYMBOLS xiii

LIST OF MAJOR ABBREVIATION xiv

ABSTRAK xix

ABSTRACT xxi

CHAPTER 1 : INTRODUCTION 1

1.1 Problem statement and motivation of the work 2

1.2 Aim and objectives 6

1.3 Highlight on the importance of the work 7

1.4 Outline of the thesis 8

CHAPTER 2 : LITERATURE REVIEW 10

2.1 Introduction to GaN material 10

2.2 Introduction to polycrystalline GaN and its applications 13

2.2.1 Choice of substrate for polycrystalline GaN 14

2.2.2 Deposition method for polycrystalline GaN 16

2.3 Improving the quality of polycrystalline GaN 20

2.3.1 Mitigation on the poor properties of polycrystalline GaN by thermal annealing 21

2.3.2 Deposition of AlN buffer layer as a strategy to improve polycrystalline GaN properties 24

2.4 Principle of metal-semiconductor-metal (MSM) photodetector 24

2.4.1 Important terminology of MSM photodetector 25

2.4.2 Polycrystalline GaN MSM photodetectors 27

2.4.3 Contacts on semiconductor material 29

2.4.4 Ohmic contact on MSM photodetector 30

2.4.5 Metal contact selection for MSM photodetector based on polycrystalline GaN 32

2.5 Summary 33

CHAPTER 3 : METHODOLOGY 35

3.1 Substrate cleaning for GaN deposition 35

3.2 Deposition of polycrystalline GaN by electron beam evaporator 37

3.3 Deposition of polycrystalline GaN by RF-sputtering 41

3.4 Post-annealing on polycrystalline GaN layer 42

3.4.1 Optimization of scrubber of annealing treatment 44

3.4.2 Controlling gas ambient of annealing treatment 45

3.4.3 Optimization of parameters of post-annealing for polycrystalline GaN 46

3.5 Characterization 48

3.5.1 X-ray diffraction (XRD) measurements 48

3.5.2 Field-emission scanning electron microscope (FESEM) measurements 50

3.5.3 Atomic force microscopy (AFM) measurement 52

3.5.4 Photoluminescence 53

3.6 Fabrication of polycrystalline GaN based metal-semiconductor-metal (MSM) photodetector 56

3.6.1 Current-voltage (IV) measurement for polycrystalline GaN based MSM photodetector 57

3.6.2 Spectral response measurement for polycrystalline GaN based photodetector 58

3.6.3 Responsivity measurement for polycrystalline GaN based photodetector 59

CHAPTER 4 : DEPOSITION OF POLYCRYSTALLINE GAN LAYERS ON M-PLANE SAPPHIRE SUBSTRATE BY ELECTRON BEAM EVAPORATOR AND RADIO FREQUENCY (RF) SPUTTERING WITH SUCCESSIVE THERMAL ANNEALING TREATMENT. 61

4.1 Deposition of GaN source by electron beam evaporator 61

4.2 Post-annealing of treatment of GaN layers on *m*-plane sapphire deposited by e-beam evaporator 65

4.2.1 Optimization of gas ambient, time and temperature on properties of GaN layer on *m*-plane sapphire 65

4.2.2 Optimization of gas flow rate on properties of GaN layer on *m*-plane substrate 79

4.3 Deposition of GaN layer by Radio Frequency (RF) Sputtering 87

4.3.1 Deposition of GaN on m-plane sapphire with different thickness using RF-sputtering 87

4.4 Effect of AlN buffer layer thickness on the properties of GaN layers deposited by RF-sputtering 91

4.4.1 Deposition of GaN layer on different thickness of AlN buffer layer 91

4.4.2 Improvement of RF-sputtering deposited GaN layer on different thickness of buffer layer by ammonia annealing treatment 96

5.4 Summary 100

CHAPTER 5: METAL-SEMICONDUCTOR-METAL (MSM) PHOTODETECTOR BASED ON E-BEAM DEPOSITED POLYCRYSTALLINE GAN 101

5.1 Current-voltage (IV) measurement using UV light source 101

5.2 Spectral responsivity 107

5.3 Temporal responsivity 109

5.4 Summary 112

CHAPTER 6: CONCLUSIONS AND FUTURE WORK 113

6.1 Conclusions 113

6.2 Future work 115

REFERENCES **117**

APPENDICES

LIST OF PUBLICATIONS

LIST OF CONFERENCES

LIST OF TABLES

		Page
Table 2.1	Low temperature emission from basal plane stacking fault (BSF) and prismatic stacking fault (PSF) of GaN material for each orientation collected from low temperature cathodoluminescence (CL) or photoluminescence (PL) method.	13
Table 2.2	Summary of morphological (SEM), structural (XRD), compositional (EDX) and optical (PL) properties along with the limitations of the techniques used for depositing polycrystalline GaN across selected literature.	19
Table 2.3	Summary of morphological (SEM), structural (XRD), compositional (EDX) and optical (PL) properties along with the limitations of the techniques used for depositing polycrystalline GaN across selected literature.	31
Table 3.1	Details of the samples deposited by e-beam evaporator, which were subjected to annealing at different time, ambient and temperature.	47
Table 3.2	Details of the GaN samples on *m*-plane sapphire substrate annealed at 950 ^{o}C for 10 minutes with different NH_3 flow rate.	48
Table 4.1	Details of the samples, which were subjected to annealing at 650 ^{o}C in N_2 or NH_3 ambient, for annealing duration of 10, 30 or 60 mins.	66
Table 4.2	Details of GaN samples, which were subjected to annealing at 950 ^{o}C.	69
Table 4.3	The N atomic % for all GaN layer deposited on *m*-plane sapphire by e-beam evaporator after annealing in different temperature, gas, and time.	70
Table 4.4	Details of GaN samples, which were subjected to annealing at 980 ^{o}C and 1100 ^{o}C in NH_3 ambient, for annealing duration of 10 mins.	77
Table 4.5	Table 4.5: Details of the GaN samples on *m*-plane sapphire substrate annealed at 950 ^{o}C for 10 minutes with different NH_3 flow rate	80
Table 4.6	Details of deposited GaN samples with different thickness by RF-sputtering	88
Table 4.7	Details of series of GaN layer grown on different thickness of AlN buffer layer.	92
Table 4.8	Details of the annealed GaN layer deposited with different thickness of AlN buffer layer by RF-sputtering.	97
Table 5.1	Details of the metal/metal oxide contact and the annealing parameters for polycrystalline GaN MSM photodetector used in this work. The contacts were deposited by RF-sputtering.	102
Table 5.2	Contact resistance for MSM photodetector samples with different contacts.	104

Table 5.3 Peak responsivity and internal quantum efficiency for the wavelengths of ~342 nm, ~385 nm and ~416 nm for MSM photodetector series used in this chapter. 109

Table 5.4 Rise time, fall time and sensitivity of MSM photodetector with different metal/metal oxide contacts. 112

LIST OF FIGURES

		Page
Figure 2.1	Atomic arrangement for wurtzite GaN with the crystal orientation axis. Each Ga atom is bonded to four neighbouring N atoms, and vice versa. Figure has been adapted from [41]	11
Figure 2.2	The planes referring to (a) *c*- (b) *m*- (c) *r*- and (d) *a*- plane inside a GaN hexagonal unit cell.	12
Figure 2.3	Epitaxial relationship between $(0001)_{sapphire}//(11\bar{2}0)_{GaN}$ and $(11\bar{2}0)_{sapphire}//(0001)_{GaN}$. Figure taken from [33]	15
Figure 2.4	The equilibrium eneregy band diagram showing the relation of *n*-type and *p*-type semiconductors with the difference between work function of the contact and the semiconductor layer. Adapted from [72]	29
Figure 3.1	Framework for this thesis	36
Figure 3.2	Schematic diagram of an electron beam evaporator used in this work	38
Figure 3.3	Process to produce GaN pellets showing (a) GaN powder, (b) schematic diagram of the moulder used to compress the GaN powder into GaN pellets, (c) GaN chunks placed on the bottom of the crucible and (d) schematic view of a loaded crucible, ready for e-beam growth.	39
Figure 3.4	Schematic diagram of sputtering system used in this work.	41
Figure 3.5	Schematic diagram for the setup of the furnace from the side view. Dimensions of the quartz tube are labeled here.	43
Figure 3.6	Schematics of a homemade HCl based scrubber system for treatment of NH_3 gas	44
Figure 3.7	Gas flow regime for an annealing time of 10 minutes for N_2 (blue line) and NH_3 (red line) gas ambient. Pre-purge, annealing, and post-purge stages are marked.	46
Figure 3.8	a) Schematic of an XRD showing the position of the x-ray tube, detector sample, the angle 2θ and ω, and b) illustration showing the **S** vector.	49
Figure 3.9	Schematic diagram of the key components inside the FESEM system used in this work.	51
Figure 3.10	Schematic diagram showing the key components of an AFM.	53
Figure 3.11	Schematics of a PL and Raman spectroscopy measurement setup used in this work.	55
Figure 3.12	(a) Schematics of the metal mask used in this work and (b) Schematics of MSM photodetector based on polycrystalline GaN showing the electrical contact	57

Figure 3.13	Schematics diagram showing the setup during IV measurements.	58
Figure 3.14	Schematic diagram showing the setup during spectral response measurements	59
Figure 3.15	3.4 V Pulses programmed into channel B of the SMU, switching the UV LED on and off for a period of 40 seconds.	60
Figure 4.1	Surface morphology of the deposited layer (a) on *m*-plane sapphire, (b) on *c*-plane sapphire.	62
Figure 4.2	XRD data of the deposited layer on *m*-plane and *c*-plane sapphire, respectively. Two diffraction peaks originate from Ga_2O_3 inclusions.	63
Figure 4.3	Relative PL spectra of the deposited layer by e-beam evaporator on *m*-plane sapphire and *c*-plane sapphire.	64
Figure 4.4	FESEM image, N atomic % composition, AFM surface morphology and surface roughness of the e-beam evaporator deposited layers annealed at 650 ^{o}C: (a) non-annealed sample, (b) Sample EM1 (c) Sample EM2, (d) Sample EM3, (e) Sample EM4, and (f) Sample EM5.	67
Figure 4.5	FESEM and AFM surface morphology of the e-beam evaporator deposited GaN layer samples annealed at 950 ^{o}C: (a) Sample EM6, (b) Sample EM7, (c) Sample EM8 and (d) Sample EM9.	68
Figure 4.6	The XRD pattern of the (a) non-annealed sample with Sample EM1 and Sample EM2, (b) Sample EM3 and Sample EM4, (c) Sample EM6 and Sample EM7, and (d) Sample EM8 and Sample EM9.	72
Figure 4.7	PL spectra of the (a) non-annealed sample with Sample EM1 and Sample EM2, (b) Sample EM3 and Sample EM4, (c) Sample EM6 and Sample EM7, and (d) Sample EM8 and Sample EM9. Note the amplification scale on the weaker spectrum. The inset in (c) shows Raman spectra for Sample EM6 and Sample EM7.	75
Figure 4.8	Surface morphology of (a) Sample EM12 and (b) Sample EM13 annealed in ammonia environment for 10 minutes at 980 ^{o}C and 1100 ^{o}C, respectively.	77
Figure 4.9	(a) XRD data of Sample EM12 and Sample EM13 and (b) PL spectrum of Sample EM12. The oscillation in the PL spectrum is due to reflection of photons on the facetted planes on its surface.	78

Figure 4.10 EDX data showing percentage of the effective N atoms that incorporated into the annealed GaN samples at 950 ^{o}C for 10 minutes at different flow rates. Also included, the N atomic percentage for the non-annealed GaN layer and a commercial GaN/*m*-Al_2O_3 for benchmarking 81

Figure 4.11 Surface morphology of GaN layer with different flow rate (a) non-annealed sample, (b) 1 slm, (c) 2 slm, (d) 3 slm and (e) 4 slm, annealed at 950 ^{o}C for 10 min at different NH_3 flow rate. Inset figure shows higher magnification image from respective samples. 82

Figure 4.12 3-D image of (a) non-annealed GaN layer, (b) Sample EM21, (c) Sample EM22, (d) Sample EM23, (e) Sample EM24, (f) dependence of surface roughness on different NH_3flow rate in GaN annealing, and (g) peak height distribution of each respective sample. 83

Figure 4.13 (a) XRD pattern of the annealed GaN at 950 ^{o}C for 10 minutes in different NH_3 flow rate. Also included is the non-annealed sample. (b) FWHM of the GaN($10\bar{1}0$), GaN (0002) and GaN ($10\bar{1}1$) peaks of the samples annealed with different NH_3 flow rate. Data for the non-annealed sample is excluded as the diffractions from GaN is not detectable. 85

Figure 4.14 PL spectra for the annealed GaN samples at 950 ^{o}C for 10 min with the variation of NH_3 flow rate. Data from non-annealed sample is not shown. 86

Figure 4.15 Dependence of GaN deposition rate by RF-sputtering on time. The square dots are the actual thickness, while the solid line is log fitting 88

Figure 4.16 XRD pattern for Sample SM5 showing its amorphous nature. 90

Figure 4.17 Surface morphology and average grains size of GaN layer for sample (a) SGM, (b) SG1, (c) SG2, (d) SG3, (e) SG4, (f) SG5 and (g) SG6 taken from FESEM measurement 93

Figure 4.18 Dependence of the surface roughness of GaN layer on thickness of AlN buffer layer. Square dots represent the surface roughness measured by AFM, while the dotted line serves as an eyeguide. 94

Figure 4.19 XRD diffraction patterns of GaN layer grown on different thickness of AlN buffer layer. 95

Figure 4.20 FESEM surface morphology and average grains size of GaN on AlN buffer layer after annealing for sample (a) SGM1, (b) SG11, (c) SG21, (d) SG31, (e) SG41, (f) SG51 and (g) SG61 98

Figure 4.21 XRD diffraction patterns for annealed polycrystalline GaN layer deposited on different AlN buffer layer thickness using *m*-plane sapphire substrate Also included is the spectrum for the GaN deposited directly onto the substrate, SGM1. 99

Figure 5.1 Dark current and photocurrent characteristics for MSM photodetector based on polycrystalline GaN deposited by e-beam evaporator from (a) Sample PD1 (b) Sample PD2 (c) Sample PD3 and (d) Sample PD4. 103

Figure 5.2 Gain calculated from ratio of photocurrent and dark current for each MSM photodetector series used in this chapter. 106

Figure 5.3 Responsivity for all MSM photodetector showing sharp response at ~342 nm, ~385 nm and ~416 nm, respectively. Inset figure shows the photoluminescence spectra of the bare polycrystalline GaN layer. 108

Figure 5.4 Temporal responsivity measurement for (a) PD1, (b) PD2, (c) PD3, and (d) PD4. The inset in (d) shows the temporal responsivity for PD4 in greater details. 110

LIST OF SYMBOLS

2θ	Incident/diffraction angle
$Å$	Angstrom
$\boldsymbol{b}$	Burgers vector
β	FWHM
c	speed of light
D_B	Threading dislocation density
e	Elementary charge of an electron
G	Gain
h	Planck's constant
I_d	Dark current
I_{ph}	Photocurrent
K	Kelvin
^oC	Degree celcius
R	Responsivity
R_c	Contact resistance
S	Sensitivity
t_f	Recovery time
t_r	Rise time
V	voltage
η	Internal quantum efficiency
λ	Wavelength
ϕ	phi axis
ω	Half of incident/diffraction angle

LIST OF MAJOR ABBREVIATIONS

AFM	Atomic force microscope
Al	Aluminum
Al_2O_3	sapphire
AlN	Aluminum nitride
Ar	Argon
Au	Gold
BSF	Basal plane stacking fault
CCD	Charge couple device
CL	Cathodoluminescence
Cryo	Cryogenic
DB	Threading dislocation density
DC	Direct current
DoE	Department of Energy
e-beam	electron beam
EDX	Energy dispersive x-ray
ETD	Everhart-Thornley detector
eV	Electron volt

FESEM	Field-emission scanning electron microscope
FWHM	Full width half maximum
Ga	Gallium
Ga_2O_3	Gallium oxide
GaN	Gallium nitride
H	Hydrogen
H_2O	Deionized water
H_2O_2	Hydrogen peroxide
H_2SO_4	Sulphuric acid
HCl	Hydrochloric acid
HeCd	Helium cadmium
HEMTs	High electron mobility transistors
HNO_3	Nitric acid
In	Indium
IR	Infrared
ITO	Indium tin oxide
IV	Current-voltage

LEDs	Light emitting diodes
MBE	Molecular beam epitaxy
MiS	metal-insulator-semiconductor
Mo	Molybdenum
MOCVD	Metal organic chemical vapor deposition
MRD	Material research diffractometer
MSM	metal-semiconductor-metal
N_2	Nitrogen
Nb	Niobium
NBE	Near band edge
NH_3	Ammonia
Ni	Nickel
Ni_xO	Nickel oxide
PA	Phase analysis
PAMBE	Plasma assisted molecular beam epitaxy
P-i-N	Positive-intrinsic-negative
PL	Photoluminescence
PLD	Pulsed Laser Deposition

PRS	Parallel receiving slit
PSF	Prismatic stacking fault
Pt	Platinum
RCA	Radio Corporation of America
RF	Radio frequency
RMS	Root mean square
SCCM	Standard cubic centimeters per minute
SEM	Scanning electron microscope
SLM	Standard liter per minute
SMU	Source measure unit
SSL	solid state lighting
Ta	Tantalum
TDs	Threading dislocations
TLD	Through lens detector
UCSB	Universiti of Santa Barbara
US	United States
USM	Universiti Sains Malaysia
UV	Ultraviolet

VLS	vapor solid liquid
W	Tungsten
XRD	X-ray diffractometer
YB	Yellow band

LAPISAN POLIKRISTAL GaN ATAS SUBSTRAT SAPPHIRE TIDAK TERKUTUB UNTUK PENDERIA FOTO LOGAM-SEMIKONDUKTOR-LOGAM

ABSTRAK

Tesis ini menghuraikan kajian memendapkan polikristal gallium nitrida (GaN) ke atas sapphire bersatah-*m* menggunakan penjimatan kos dari teknik pemendapan fizikal; penyejatan pancaran elektron (e-beam) dan percikan frekuensi radio (RF), diikuti dengan penyepuhlindapan dalam persekitaran gas amonia (NH_3). Kajian ini diteruskan dengan penghasilan penderia foto logam-semikonduktor-logam (MSM) bersama dengan sesentuh logam/logam oksida yang paling sesuai bagi menambah baik kecekapan peranti tersebut. Bahagian awal tesis ini menghuraikan kajian penambahbaikan ciri ciri lapisan polikristal GaN yang dimendapkan menggunakan penyejatan e-beam dengan mengawal gas persekitaran, masa, suhu, dan kadar aliran gas bagi rawatan penyepuhlindapan tersebut. Sebelum penyepuhlindapan dilakukan, lapisan GaN tersebut mengandungi gallium oksida (Ga_2O_3) dengan peratusan atomik N yang sedikit. Semasa penyepuhlindapan berlaku, sebahagian daripada Ga_2O_3 tersebut telah keluarkan, sementara penghabluran semula butiran GaN terjadi, dan kekurangan-N didalam lapisan polikristal GaN dipulihkan. Keadaan penyepuhlidan terbaik didapati pada 950 ^oC selama 10 minit dengan kadar aliran NH_3 pada 3 slm. Lapisan GaN yang disepuhlindap dengan keadaan terbaik menunjukkan pembentukan butiran dengan struktur berfaset heksagonal yang lebih besar, beserta tiga puncak pembelauan GaN yang tirus dan berbeza bersepadan dengan orientasi $(10\bar{1}0)$, (0002) dan $(10\bar{1}1)$. Selain itu, perubahan positif yang ketara bagi pancaran berhampiran pinggir jalur (NBE) diperhatikan. Pemendapan lapisan

polikristal GaN juga telah dilakukan menggunakan percikan-RF, tertumpu pada kawalan ketebalan lapisan penampan aluminum nitride (AlN) sebelum disepuhlindapkan dengan keadaan terbaik seperti yang telah dihuraikan. Lapisan polikristal GaN yang dimendapkan diatas lapisan penampan AlN 70 nm menunjukkan keputusan yang terbaik dari data XRD, berbanding yang lain. Sampel-sample yang lain didalam set ini tidak menunjukkan keputusan yang baik dari pengukuran permukaan dan optikal. Oleh itu, lapisan polikristal GaN yang dimendapkan dengan penyejatan e-beam adalah lebih baik berbanding dengan percikan-RF, dan boleh dibangunkan sebagai penderia foto MSM. Bagi meningkatkan kecekapan penderia foto berasaskan polikristal GaN, sesentuh elektrikal bagi peranti ini telah dioptimumkan. Disini, sesentuh berbeza dikaji: aluminum (Al), oksida-timah-indium (ITO), nikel (Ni) dan platinum (Pt). Penderia foto berasaskan polikristal GaN yang terbaik telah didapati dengan penggunaan sesentuh Ni pada λ=385 nm. Peranti ini menunjukkan arus foto-terjana ~900 nA/cm^2 pada 5 V, dengan perolehan ~100 pada voltan ~1.5 V - ~4.0 V. Penderia foto MSM ini menunjukkan kerintangan, kecekapan kuantum dalaman, masa naik, masa pemulihan dan sensitiviti masing-masing pada 2.02 MΩ.cm^2, 3.13%, 1.75 saat, 1.87 saat, dan 5840 %. Ini disebabkan pembentukan kemasukkan Ni_xO, yang memberikan prestasi yang lebih baik pada penderia foto tersebut.

POLYCRYSTALLINE GaN LAYER ON NON-POLAR SAPPHIRE SUBSTRATE FOR METAL-SEMICONDUCTOR-METAL PHOTODETECTOR

ABSTRACT

This thesis describes work on depositing polycrystalline gallium nitride (GaN) on *m*-plane sapphire substrate using cost effective physical deposition technique; electron beam (e-beam) evaporator and radio frequency (RF) sputtering, followed by annealing treatment in ammonia (NH_3) ambient. The work was then extended to develop metal-semiconductor-metal (MSM) photodetector using the most possible metal/metal oxide contact, to increase the efficiency of the device. The initial part of this thesis focus on ameliorating the properties of the polycrystalline GaN layer by controlling gas ambient, time, temperature, and gas flow rate of the annealing treatment. Before the annealing, the layer consisted of gallium oxide (Ga_2O_3) inclusions, with low nitrogen (N) atomic percentage. During the annealing, the Ga_2O_3 inclusions were partially removed, while recrystallization of the GaN grains occurred and the N-deficiency in the polycrystalline layer was mitigated. The best annealing condition was found at 950 ^oC with the duration of 10 minutes with the NH_3 flow rate of 3 slm. The GaN layer annealed with the best condition showed the formation of larger hexagonal facetted structure, accompanied by three narrow and distinct GaN diffraction peaks corresponding to $(10\bar{1}0)$, (0002) and $(10\bar{1}1)$ orientations. Furthermore, a significant optical improvement of the GaN related near band edge (NBE) emission was observed. Deposition of polycrystalline GaN layer by RF-sputtering was also conducted, focusing on controlling the thickness of aluminum nitride (AlN) buffer layer prior to annealing with the best condition as

described before. The polycrystalline GaN layer deposited on 70 nm AlN buffer layer showed the best results from the XRD data, as compared to others. All other samples in this set did not exhibit promising results from surface and optical measurements. Therefore, the polycrystalline GaN layer deposited by e-beam evaporator is better than one by RF-sputtering, and worth to be developed as MSM photodetector. In order to increase the efficiency of the polycrystalline GaN based photodetector, the electrical contact of the device was optimized. Here, different contacts were studied; aluminum (Al), indium-tin-oxide (ITO), nickel (Ni), and platinum (Pt). The best polycrystalline GaN based MSM photodetector was found with the use of Ni contact at λ=385 nm. This device exhibited photo-generated current of ~900 nA/cm^2 at 5 V, with a gain of ~100 between the bias voltage of ~1.5 V – ~4.0 V. The MSM photodetector showed contact resistivity, internal quantum efficiency, rise time, recovery time and sensitivity of 2.02 MΩ.cm^2, 3.13%, 1.75 sec, 1.87 sec, and 5840 %, respectively. This behavior was related to the formation of Ni_xO inclusions, which subsequently gave better efficiency to the photodetector.

CHAPTER 1

Introduction

Recent motivation towards solid state lighting (SSL) has been driven by the opportunity to establish energy efficiency lighting source, which would replace conventional incandescent and compact fluorescent lamps. A projection by the United States (US) Department of Energy (DoE) has listed an annual electricity consumption saving from general illumination application of 395 TWh by 2030 [1]. In order to achieve this target, 88% from the total lumen-hours by general illuminations should consist of SSL devices. Despite of the DoE's effort in the assisting the influx of SSL devices, the adoption rate for SSL in the US is stagnant at 6.8% in 2015. This is mainly due to the high initial cost of ownership for solid state SSL devices, which discourages adoption. With this in mind, tremendous endeavor on a global scale has been made in driving up efficacy and manufacturing scale, while scaling the price down in order to realize the projected energy saving.

Gallium nitride (GaN) semiconductor material and its family of alloys are rapidly becoming the prevalent compound semiconductors not only for light emitting diodes (LEDs) SSL device, but also for photodetector application. This is largely attributed to the tunable band gap of its ternary alloys, which covers mid-ultraviolet (UV) up to infrared (IR) section in the electromagnetic spectrum. This enables the study of lighting from a single light source for psychological responses to improve well-being, to increase productivity and to minimize negative effects of artificial lighting on human, animal and even plants. Moreover, the electrical robustness and built-in polarization of GaN semiconductor material has found application in niche area of power devices, such as the high mobility electron transistors (HEMTs). Furthermore, GaN has a high breakdown voltage, which is beneficial for high-

powered devices, and devices with smaller dimension. Not to mention, GaN based material is able to operate in extreme temperature due to its thermal stability.

Traditionally, single crystal GaN is grown along the polar *c*-plane direction [2]. In the recent years, there is a shift in research motivation that has grown single crystal GaN in non-polar and semi-polar orientations. This is mainly driven by the effort to reduce the drooping effect in LEDs under high electric field, which is dominant for nitrides LEDs grown in polar *c*-plane direction. Since GaN can be grown in various orientations, this opens up the possibility for polycrystalline GaN structure, in addition to the common single crystal structure. In photodetector technology, polycrystalline GaN based on it has the potential to detect light at a wider range of wavelength as compared to its counterpart in single crystal structure.

1.1 Problem statement and motivation of the work

The first concern is the method to develop material for the photodetector. Metal organic chemical vapor deposition (MOCVD) and molecular beam epitaxy (MBE) are well known methods for growing GaN material [3-8]. Metal-semiconductor-metal (MSM) photodetectors in GaN material, which were developed from these techniques typically exhibit rapid response to light excitation [4, 5, 7, 8], where the typical range is 20 ns – 760 ns. Nonetheless, it was found that these MSM photodetectors often have a responsivity in the range of 0.0012 A/W – 0.1830 A/W, which is similar to a recent report, where thermal vapor evaporated GaN was used to develop GaN material [9] and has a responsivity of 0.28 A/W. From this survey, it should be considered that thermal vapor evaporation method is the more cost effective method, than MOCVD or MBE. The survey also implies that an expensive and sophisticated techniques are not necessary for GaN material deposition to develop as a MSM photodetector. For this reason, recent attentions have been given

to radio frequency (RF) sputtering [10, 11], and thermal vapor deposition [9] as a tool to develop GaN based MSM photodetector. Nevertheless, the potential of MSM photodetector in GaN material using electron beam (e-beam) evaporator has yet to be demonstrated. E-beam evaporator has been reported to give better surface to the deposited material, as compared to RF-sputtering and thermal vapor deposition [12].

Polycrystalline GaN is attractive material for UV photodetector application [13], which is capable of detecting the wavelengths in the range of 280 nm – 410 nm [7, 8, 14]. In comparison, the detection for a photodetector based on single crystal GaN is limited at ~360 nm [6, 15-18]. Despite of this, this research area has not gained much attentions due to the presence of grain boundaries in the polycrystalline material, causing poor electrical properties to the photodetector based on it [19]. This is a challenge that is worth to take in order to explore the potential of polycrystalline GaN for better device development.

Throughout the years, several methods have been proposed for polycrystalline GaN deposition, such as pulsed laser deposition (PLD) [20], electrodeposition [21, 22], sol-gel [23-25], magnetron sputtering and RF-sputtering [26, 27], and electron beam (e-beam) evaporator [28]. Nonetheless, the deposition time of the PLD technique is limited, whereas the properties of the precursors for sol-gel and electrodeposition technique are sensitive to the humidity and temperature of the surrounding. On the other hand, techniques such as magnetron sputtering and RF-sputtering, and e-beam evaporator could to be the possible technique for polycrystalline GaN deposition. Nonetheless, both techniques come with their set of advantages and disadvantages. For the sputtering system, group V source can be easily introduced as its design can easily accommodate N_2 gas source. However, due to the non-flexible nature of magnetron sputtering and RF-sputtering the deposition

rate of this technique is low (a few nm/min in this work). Furthermore, the extended period of deposition will risk the surface damage of the polycrystalline GaN from the oscillating plasma. On the other hand, e-beam evaporator is able to provide a faster deposition rate (up to ~12.0 nm/min in this work). However, due to the isolated design nature of e-beam evaporator, introducing N plasma during the deposition is difficult. In addition, both techniques tend to produce insufficient polycrystalline GaN crystal quality due to their low in-situ annealing temperature.

Therefore, improving the material quality of the polycrystalline GaN layer via post-annealing process is an alternative solution to the above issue. It has been demonstrated that the post-annealing process promotes recrystallization to the polycrystalline GaN layer, thus eliminates threading dislocations (TDs) in the grains boundaries. The annealing parameters; i.e.: ambient, time, temperature and gas flow rate play important role. It is expected that the proper gas ambient is able to mitigate N-deficiency in the GaN layer, while the appropriate annealing time could promote sufficient recrystallization process while preventing GaN grains loss. Meanwhile, the annealing temperature is expected to provide thermal energy for the recrystallization. Finally, the gas flow rate determines the effectiveness of active N species to incorporate into the polycrystalline GaN lattice structure. Specific investigation on the relationship between gas flow rate and reduction of N deficiency has yet to be demonstrated.

Another common method to improve GaN layer in general is by introducing aluminum nitride (AlN) buffer layer. This layer reduces stress through the reduction of misfit dislocations [29] and subsequently improves the deposition of the overlying layer [30]. Nonetheless, the thickness of the AlN buffer layer can influence the material quality of the GaN and hence to the device. If the AlN buffer layer were too

thin its ability as described above will be insignificant. On the other hand, AlN with larger thickness will serve as insulative material, subsequently affect the electrical injection to the device.

The choice of substrate plays an essential role to promote successful deposition of polycrystalline GaN. Using the conventional *c*-plane sapphire has resulted in inconsistency in the orientation of polycrystalline GaN [31] and non-uniform layer [32]. Meanwhile, deposition of GaN layer on Si(111) has resulted in single crystal structure [20]. Selecting polycrystalline metal substrate such as tungsten (W), molybdenum (Mo), tantalum (Ta) and niobium (Nb) substrates have included various GaN orientations. On the other hand, several research groups have identified that GaN layer can be grown in multiple orientations on *m*-plane sapphire substrate [33-38]. These reports mainly focused on the effect of growth condition on the relationship of the GaN layer. Later, it was reported that *m*-plane has the ability to force GaN layer to grow in its orientation, but the layer contains high density of basal plane and prismatic stacking fault [34, 39, 40]. From this observation, there is a possibility to manipulate such behavior that would give advantage to polycrystalline GaN in the end.

For example, MSM photodetector based on polycrystalline GaN was reported to detect light at a much wider wavelength range [7, 8, 14] than single crystal GaN based MSM photodetector [6, 15-18]. Previous work by [3] demonstrated that their MSM photodetector grown on porous alumina buffer layer exhibited slow rise and recovery time, possibly due to the material quality of the polycrystalline GaN. It is suspected that the surface of the porous alumina created a series of perturbation in the boundary layer in the growth reactor chamber, which subsequently affects the growth kinetics of the GaN layer. Recent polycrystalline based MSM photodetector

deposited by thermal vapor deposition method exhibits low sensitivity [9], which is suspected to originate from the non-optimal deposition temperature, affecting the polycrystalline GaN structure. It is now apparent that improving the quality of the GaN layer is important to achieve the best performance out of the MSM photodetector based on such material.

This work will focus on improvement of polycrystalline GaN deposited on *m*-plane sapphire substrate by using e-beam evaporator and RF-sputtering, with successive post-annealing treatment. The optimizing conditions for the post-annealing treatment will be focused on gas ambient, time, temperature and gas flow rate. Later, surface morphology, nitrogen elemental composition, crystal stricture and optical properties will be evaluated with respect to variation of the post-annealing conditions. The work continues with development of MSM photodetector with the variation of metal/metal oxide contacts to improve the electrical performance of the photodetector.

1.2 Aim and Objectives

In brief, this work focuses on depositing polycrystalline GaN layers by e-beam evaporator and RF-sputtering, with successive annealing treatment. The best sample will be fabricated into functional MSM photodetector with the variation of electrical contact. The sufficient quality polycrystalline GaN based MSM photodetector will be demonstrated for the first time.

The objectives of this project are:

1. to determine the preferable deposition technique for polycrystalline GaN

2. to define the optimum post-deposition treatment for improving crystal quality of the polycrystalline GaN (i.e. gas ambient, time, temperature and flow rate)
3. to proof the improved polycrystalline GaN can function as a MSM photodetector.

1.3 Highlight on the importance of this work

The highlight of this thesis is included as the following points:

1. Due to its poor electrical property, research activities have given little attention on polycrystalline GaN structure, as most effort favors its single crystal counterpart. So far, devices based on polycrystalline GaN layers deposited by cost-effective techniques have yet to be demonstrated, and its potential is yet to be explored. In this work, polycrystalline GaN layer with sufficient quality has been successfully deposited using e-beam evaporator. This layer is later fabricated into a pioneering MSM photodetector based on polycrystalline GaN deposited by a cost-effective method.
2. This work includes effort to significantly improve the properties of the polycrystalline GaN layer through optimization of post-annealing parameters.
3. The study which relates the nitrogen deficiency with the flow rate of ammonia gas during annealing is shown and is addressed in this work.
4. To the best of my knowledge, fabricating MSM photodetector on sufficient quality polycrystalline GaN layer deposited e-beam evaporator has not been done so far, and is therefore demonstrated in this work. The

MSM photodetector based on polycrystalline GaN here shows a high sensitivity for detection of light at the wavelength of 385 nm.

1.4 Outline of the thesis

This thesis is organized as the following:

Chapter 2 will discuss published works on producing polycrystalline GaN. Critical judgements on the related techniques that have been performed to produce the polycrystalline GaN layer will be included. The proposed technique to produce polycrystalline GaN will be discussed, along with its advantages over previous techniques. This is followed by progress in developing MSM photodetector based on nitrides materials.

Chapter 3 gives details of experiments, including preparation for the deposition using e-beam evaporator and RF-sputtering. Description of conducting annealing with different ambient, time, temperature and gas flow rate hence to follow. Next, deposition details of Al, ITO, Ni and Pt contacts by RF-sputtering for the fabrication of MSM photodetector will be described. Further, the information of related characterization techniques used throughout this work will be discussed. Problems and issues that were encountered throughout this work are given, and followed by proposed solutions.

Chapter 4 will focus on deposition of GaN layers on *m*-plane sapphire substrate by e-beam evaporator with successive thermal annealing treatment. More particularly, the properties of polycrystalline GaN layer deposited on *m*-plane sapphire by e-beam evaporator will be first characterized from the aspect of surface morphology, nitrogen elementary composition, crystallography, and optical measurements.

Subsequently, the effect of post-annealing conditions; i.e. gas ambient, time, temperature and flow rate on the properties of the GaN layers will be discussed.

Chapter 5 will focus on deposition of polycrystalline GaN layer by RF-sputtering, primarily changing the thickness of AlN buffer layer of the GaN layer. The optimized annealing conditions, as established in Chapter 4 will be applied in this case. The effect of AlN buffer layer thickness on the surface morphology, and crystallography of the polycrystalline GaN layer will be described. At the end of the chapter, the properties of polycrystalline GaN deposited by e-beam evaporator and RF-sputtering will be compared, and the best polycrystalline GaN layer will be proposed to be fabricated into functional MSM photodetector.

Chapter 6 will primarily discuss the electrical characteristics of MSM photodetector based on the best polycrystalline GaN as proposed in the previous chapter. The MSM photodetector will be fabricated by using Al, ITO, Ni and Pt contacts. The current-voltage IV (contact resistance and gain), spectral response (responsivity and internal quantum efficiency) and temporal response (rise time, recovery time and sensitivity) properties of the MSM photodetectors with different metal contacts will be discussed. At the end of the chapter, the most possible metal contact for MSM photodetector based on polycrystalline GaN will be proposed.

Chapter 7 will summarize the finding of this work. This is followed by suggestions for future work that can be done to further improve the quality of this work.

CHAPTER 2

Literature Review

This chapter will give a brief introduction to gallium nitride (GaN) material and specifically followed by the introduction and motivation of GaN in polycrystalline structure. Next, review on deposition methods that have been used for depositing polycrystalline GaN will be given. This will justify the proposed method performed in this work, including adopting advantages of thermal annealing as attempts to improve the properties of the polycrystalline GaN after the deposition, including the insertion of AlN buffer layer for polycrystalline GaN. Subsequently, the basic principal and selection of metal/metal oxide contacts for polycrystalline GaN based metal-semiconductor-metal (MSM) will be discussed.

2.1 Introduction to GaN material

Gallium nitride (GaN) is a semiconductor material, that has potential for producing great devices. With a wide and direct band gap of 3.4 eV, GaN is a suitable material to fabricate optoelectronic devices such as light emitting diodes (LEDs), lasers, and photodiodes, which can operate at high temperature, power and frequency. Furthermore, strong polarization field along its *c*-plane direction is suitable for high frequency devices such as high electron mobility transistors (HEMT). Recently, Universiti Sains Malaysia (USM) and University of California Santa Barbara (UCSB) through Collaborative Research in Engineering Science and Technology (CREST) have reached an agreement for transferring technology of developing high-brightness and high-efficiency LEDs in Malaysia. It is a large scale investment of the Malaysian government to develop nitride epitaxy and talent in the country.

Generally, GaN could be formed into wurtzite (hexagonal) or zinc-blende (cubic) phases. Hexagonal GaN is thermodynamically stable, whereas cubic GaN is metastable in nature. The hexagonal unit cell in figure 2.1 shows each Ga atom is bonded to four neighboring nitrogen (N) atoms, and vice versa. A hexagonal GaN crystal structure contains two different lattice constants, where *a* corresponds to the distance between atoms in a basal planes, whereas lattice constant *c* corresponds to the distance between two nearest basal planes. The stacking sequence configuration for wurtzite GaN in <0001> direction is ABABAB, whereas a zinc-blende GaN in <111> direction is ABCABC. Here A corresponds to Ga^{3+} cation while B corresponds to N^{3-} anion.

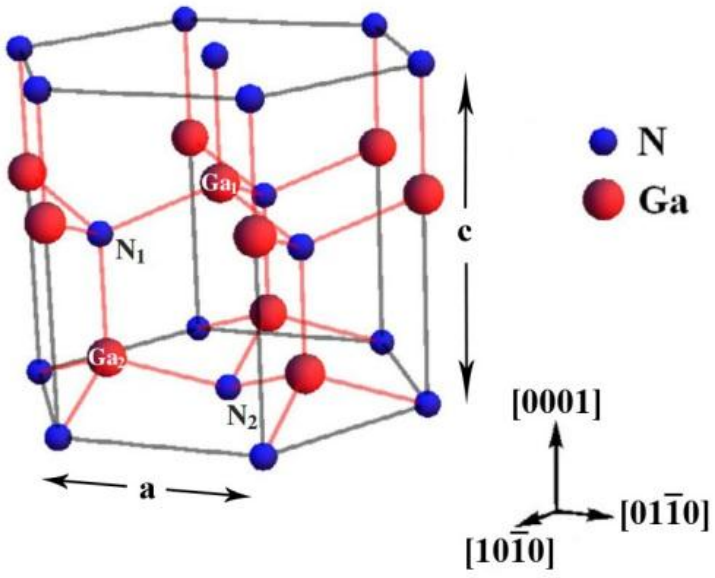

Figure 2.1: Atomic arrangement for wurtzite GaN with the crystal orientation axis. Each Ga atom is bonded to four neighbouring N atoms, and vice versa. Figure has been adapted from [41].

GaN can be grown in several orientations. Since the early 1990s, most of the GaN and its devices have been grown in *c*-plane orientation [2]. This is the plane perpendicular to [0001] direction, as shown by the shaded region in figure 2.2 (a). In

extension, GaN also can be grown in $(10\bar{1}0)$, $(10\bar{1}1)$ and $(11\bar{2}0)$ orientations, which is known as *m*-, *r*- and *a*-planes, respectively, see figure 2.2 (b)-(d). Fault in the stacking sequence of the GaN layers has been identified by type I_1 basal plane stacking fault (BSF) and type I_2 prismatic stacking fault (PSF). The difference between both types of stacking faults is that the vector for BSF is perpendicular to the growth surface, whereas the vector for PSF typically lies along $\frac{1}{2}(10\bar{1}1)$. Both types of stacking fault has a ABABCBC configuration. Notice the presence of both

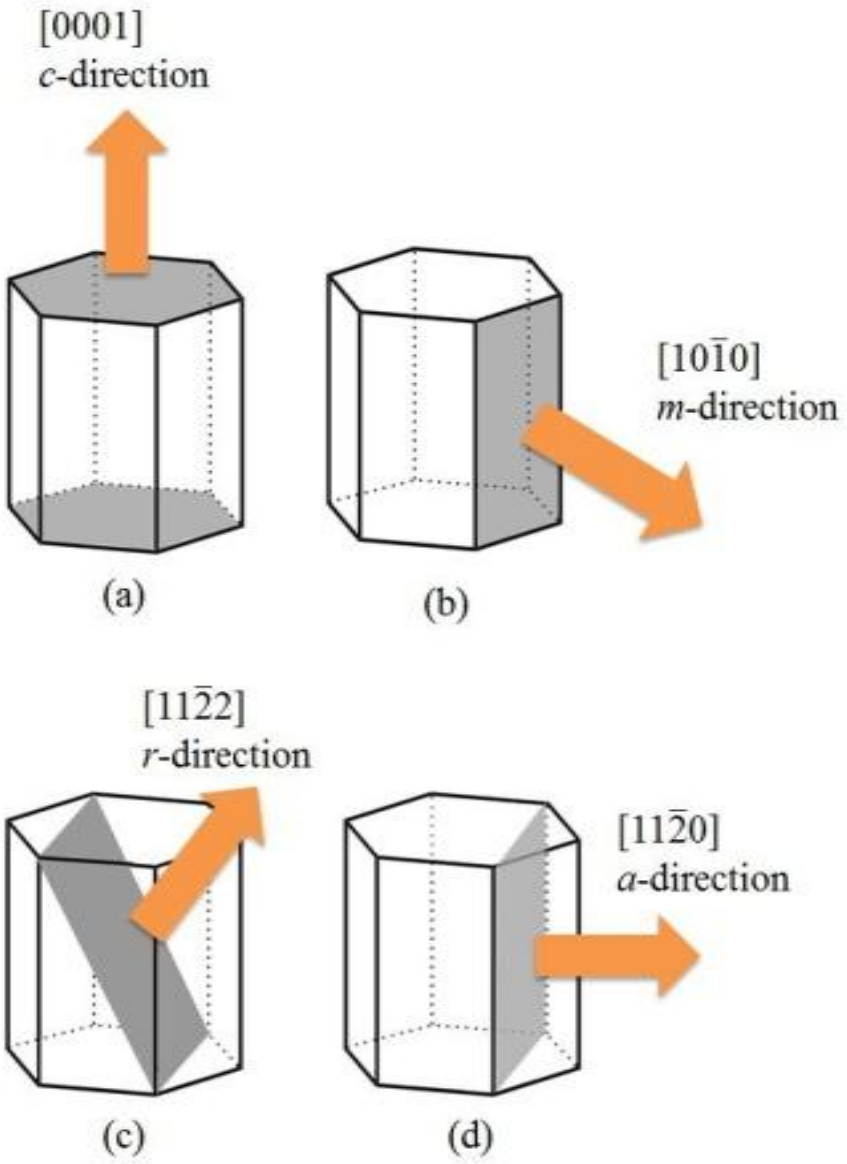

Figure 2.2: The planes referring to (a) *c*- (b) *m*- (c) *r*- and (d) *a*- plane inside a GaN hexagonal unit cell.

wurtzite and zinc-blende phases in the stacking fault. This would usually result in sandwiching of zinc-blende phase in between two wurtzite phases. The 'fingerprint' luminescence emission of both BSF and PSF are listed in Table 2.1.

Table 2.1: Low temperature emission from basal plane stacking fault (BSF) and prismatic stacking fault (PSF) of GaN material for each orientation collected from low temperature cathodoluminescence (CL) or photoluminescence (PL) method.

GaN plane orientation	Literature	Method	Temperature (K)	Optical emission (eV)	
				BSF, Type I_1	PSF, Type I_2
a-GaN	[42]	CL	5	3.14	3.33
m-GaN	[39]	PL	12	3.42	3.34
r-GaN	[43]	PL	13	3.42	3.32
c-GaN	[44]	PL	6	3.44	Not provided

2.2 Introduction to polycrystalline GaN and its applications

Research on polycrystalline GaN material has not been gained much attention as its single crystal counterpart throughout the years due to the presence of grain boundaries, which may cause poor electrical properties to the device based on it [19]. Nonetheless, polycrystalline GaN has a big potential for UV photodetector application [13] as compared to single crystalline GaN. This is because it is capable of detecting wider wavelengths from 280 nm – 410 nm [7, 8, 14], whereas photodetectors based on single crystal GaN has limited wavelength detection at ~360 nm [6, 15-18]. Polycrystalline GaN is mainly grown in (0002), $(10\bar{1}0)$ and $(10\bar{1}1)$ orientations [19, 20, 26]. However, in some cases, small inclusions of GaN in other orientations also have been observed [27, 28, 45, 46].

2.2.1 Choice of substrate for polycrystalline GaN

Generally, *c*-plane sapphire substrate is only suited to single crystal GaN in (0002) orientation [47, 48] and therefore is not preferable for growing polycrystalline GaN. This is due to the lower surface energy of the plane and the matching of crystal symmetry of *c*-plane sapphire with GaN (0002). Without proper growth condition, attempts to produce polycrystalline GaN on *c*-plane sapphire substrates have resulted in inconsistencies of the orientations [31] and also severe variation of the morphologies and film thickness throughout the surface [32]. This will cause inconsistency on the performance of the polycrystalline GaN device that is fabricated on a *c*-plane substrate.

It is obvious that another suitable candidate should be evaluated for deposition of polycrystalline GaN. Growing GaN on *m*-plane sapphire substrates have been demonstrated by several research groups [33-38]. Unlike the growth of *c*-plane GaN/*c*-plane sapphire, which only takes the lattice mismatch into account, the growth of GaN/*m*-plane sapphire will consider the surface energy and interfacial energy [33] in addition to domain matching mechanism [49]. As presented in figure 2.3, for the GaN/*m*-plane sapphire with $(0001)_{sapphire}//(11\bar{2}0)_{GaN}$ and $(11\bar{2}0)_{sapphire}//(0001)_{GaN}$ epitaxy relation, the lattice mismatch are 26.23% and 9.17% respectively [33]. At first, it seems that growth of GaN on *m*-plane sapphire is not favorable due to the unusually high lattice mismatch. However, after considering the domain matching epitaxy mechanism for epitaxial layer with large lattice mismatch [49], it was found that that the growth for GaN layer on *m*-plane sapphire is dictated by GaN (0002) and sapphire $(10\bar{1}4)$ planes, with a lattice mismatch of. ~1.8% [33]. Lattice mismatch for common sapphire and GaN planes is provided in Appendix A. This property is the reason for the dense basal plane and prismatic stacking fault

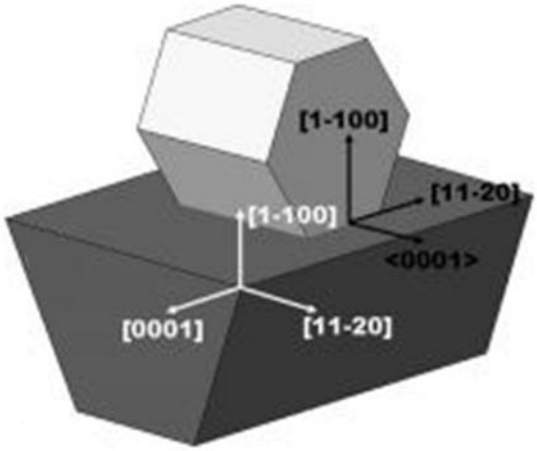

Figure 2.3: Epitaxial relationship between $(0001)_{sapphire}//(11\bar{2}0)_{GaN}$ and $(11\bar{2}0)_{sapphire}//(0001)_{GaN}$. Figure taken from [33]

when *m*-plane GaN is forced to grow on *m*-plane sapphire [34, 39, 40]. This factor limits the ability to grow high quality single crystalline *m*-plane GaN/*m*-plane sapphire. However, this limitation has the advantage to further strengthen the potential of *m*-plane sapphire substrates to grow polycrystalline GaN, even without any presence of buffer layer. Thus, GaN layer grown in $(1\bar{1}00)$ [33, 35, 36], $(10\bar{1}0)$ [37, 38], $(1\bar{1}03)$ [33, 34, 37], $(11\bar{2}0)$ [38] and $(11\bar{2}2)$ [33, 34] have been reported to be grown on *m*-plane sapphire. Nevertheless, other GaN orientations that may also present as the role of surface and interfacial energy on the orientation of the GaN layer is not well understood, even when quasi-equilibrium studies have been conducted [50].

There have also been efforts to grow polycrystalline GaN on substrates other than sapphire. Earlier attempt to grow polycrystalline GaN on Si (111) substrates have resulted in (0002) GaN layer orientation [20]. This is expected as the three-folded symmetry of Si (111) serves as a template for growth of GaN in that particular orientation, while suppressing GaN formation in other directions. Interestingly, the

crystal symmetry of the substrate should be different than the GaN for a good polycrystalline GaN structure, as proposed in [33]. The report demonstrated that a rhombohedral SiO_2 substrate successfully grew GaN in polycrystalline structure [27]. The polycrystalline GaN was deposited using magnetron sputtering, but poor optical emissions were observed due to surface damage on the GaN layer by plasma. Using a polycrystalline metal substrate (i. e.: tungsten (W), molybdenum (Mo), tantalum (Ta) and Niobium (Nb)) for the growth of polycrystalline GaN resulted in a mixture of wurtzite and zinc-blende phases [51]. The presence of both phases of GaN is a strong indication of the presence of dense stacking fault in the polycrystalline GaN layer [52]. Apart from that, metal substrates are malleable and this would inflict stress on the brittle GaN layer. Therefore, metal substrates are not suitable for devices based on polycrystalline GaN. In this work, *m*-plane sapphire is proposed as the substrate for the polycrystalline GaN, since the atom arrangement in this plane is not prone to the GaN growth even in $(10\bar{1}0)$ direction [33, 53]. Furthermore, *m*-plane sapphire still retains the similar chemical and physical robustness to *c*-plane sapphire, which makes it suitable for devices to operate at extreme conditions.

2.2.2 Deposition method for polycrystalline GaN

In order to evaluate the best deposition method for polycrystalline GaN, several selected techniques will be discussed here. Initially, pulsed laser deposition (PLD) system was used to deposit polycrystalline GaN [20]. This technique utilizes an external laser source aimed at a GaN target through a quartz window. The disadvantage is obvious when a zinc oxide (ZnO) buffer layer is needed to promote a better structural property for the polycrystalline GaN layer. Nonetheless, the surface morphology shows irregular size distribution of hexagonal facetted structure. On the other hand, utilizing magnetron sputtering [27] or radio frequency (RF) sputtering

[26] has been reported to produce good polycrystalline structure. From their surface morphology, it was found that polycrystalline GaN deposited by magnetron sputtering has exhibited better formation and distribution of hexagonal facetted structure as compared to RF sputtering. Regardless, magnetron sputtering uses Ga metal as the source and therefore risking deposition of the Ga metal itself on the substrate [26]. Furthermore, the intensity for GaN related near band edge (NBE) emission in the photoluminescence spectrum is poor.

Chemical deposition for polycrystalline GaN also has been utilized in the past. Sol-gel method for deposition of polycrystalline GaN previously managed to produce polycrystalline GaN, with a near stoichiometric Ga:N composition ratio [23]. In this case, the polycrystalline GaN deposition was successful because no substrate was used, and therefore, GaN are free to form in multiple orientations. However, without a sufficient density, it was found difficult for handling and future processing. Furthermore, this technique is prone to produce nanotubes [54], which causes a red-shift of the GaN related NBE emission to ~390 nm. To address this issue, viscous sol-gel precursors were first deposited on a substrate, before the substrate was placed on a spin-coater. Similar to sol-gel method, the Ga:N composition ratio is reported to be near stoichiometric. Moreover, this method has managed to exhibit well-formed and uniform distribution of hexagonal facetted structure. However, sol-gel spinning only manage to produce highly oriented GaN in (0002) direction, with very little inclusions of GaN in $(10\bar{1}0)$ and $(10\bar{1}1)$ directions [24, 25]. Moreover, thickness of the GaN layer depends on the precursor viscosity and homogeneity, spinning duration, and speed of the spin coater. Thus, thickness uniformity is hardly controllable using this technique. Electrodeposition technique also has yielded successful deposition of polycrystalline GaN. However,

electrodeposition risks contaminating the GaN layer with byproducts from the precursor [21], exhibited poor surface morphology without hexagonal facetted structure [21], and a successful electrodeposition of polycrystalline GaN requires an extended duration for proper deposition [22]. Even though sol-gel spinning and electrodeposition technique have the potentials for depositing polycrystalline GaN, the precursor property is very sensitive to the changes in humidity and temperature of the environment, not to mention the time consuming process for preparation. Going for electron beam (e-beam) evaporator as the alternate deposition technique for polycrystalline GaN [28] has resulted in an irregular surface morphology, and hence it is not suitable for device fabrication. This is attributed to the low in-situ annealing temperature of the heating element in an e-beam system. This issue can be easily overcome by proposing an ex-situ annealing on the polycrystalline GaN layer. Table 2.2 summarizes the results from x-ray diffraction (XRD), energy dispersive x-ray (EDX) spectroscopy and photoluminescence (PL) and limitations of the techniques as been discussed here.

In addition, using metal organic chemical vapor deposition (MOCVD) to grow polycrystalline GaN also has been reported in [19]. However, even after tuning the growth recipe for polycrystalline growth, the GaN from this technique still produces a highly oriented GaN layer [45]. In principle, MOCVD is a specialized technique to specifically grow high quality single crystal layers.

This work will propose to utilize radio frequency (RF) sputtering and e-beam evaporator to deposit polycrystalline GaN layer on *m*-plane sapphire. As compared to other techniques as described in Table 2.3, RF-sputtering and e-beam evaporator are chosen in this work because both are affordable and can offer easy operation.

Table 2.2: Summary of morphological (SEM), structural (XRD), compositional (EDX) and optical (PL) properties along with the limitations of the techniques used for depositing polycrystalline GaN across selected literature.

Method	FESEM	XRD	EDX	PL	Limitations	Ref.
PLD	Irregular size distribution of hexagonal facetted structure	Polycrystalline GaN with high orientation towards (0002) direction			Requries ZnO buffer layer	[20]
RF-sputtering	Hexagonal facetted structure with poor symmetry	Good polycrystalline structure with inclusion of Ga diffraction			Ga metal is unintentionally deposited on the substrate	[26]
Magnetron sputtering	Good formation and distribution of hexagonal facetted structure			GaN related NBE emission exhibits poor intensity		[27]
Sol-gel		Polycrystalline GaN deposited at various orientation	Near stoichiometric composition Ga:N ratio	Emission observed at ~390 nm, indicating defective GaN structure	Polycrystalline GaN too fragile and prone to growth of nanotubes	[23]
Sol-gel spinning	Good formation and distribution of hexagonal facetted structure	Polycrystalline GaN with high orientation towards (0002) direction	Near stoichiometric composition Ga:N ratio		Low control on uniformity of polycrystalline GaN layer	[24, 25]
Electro-deposition	Poor surface morphology. Does not exhibit any hexagonal facetted structure	Polycrystalline GaN structure contains diffraction from electrolyte contamination			Extended duration of deposition time	[21, 22]
E-beam deposition	Irregular surface morphology	Polycrystalline GaN structure		GaN related NBE emission is blue shifted.	Low in-situ annealing temperature	[28]

Secondly, all equipment parts needed for deposition is self-contained inside the growth chamber, unlike PLD systems. Nonetheless, the reported polycrystalline GaN deposited from both techniques are usually far from expected. Therefore, this work will propose possible solutions to the issue.

2.3 Improving the quality of polycrystalline GaN

In general, the crystal quality of the deposited polycrystalline GaN by RF-sputtering and e-beam evaporator is limited by the low deposition temperature of the systems. Hence, it is proposed that a successive post-annealing treatment should be carried out. In general, the quality of a GaN layer is related to the threading dislocation (TDs) density present in the layer. A previous study has correlated the effect of thickness and stress with the quality of the GaN layer [55]. A thicker GaN layer was found to contain a reduced TD density due to the reduction of residual stress. In turn, the quality of the GaN layer is expected to improve with increase in thickness. Since there is little work for the estimation of TDs density on polycrystalline structures, the well-known model based on single crystal will be referred here instead. The TDs density can be estimated by the full width half maximum (FWHM) of its respective x-ray diffractometer diffraction peak. For a highly defective nitride layer, the dislocation density is related directly to the lattice twist and tilt [56]. Since TDs are formed at the grains boundary, the TDs density (D_B) can be approximated by [57]:

$$D_B \approx \frac{\beta^2}{4.35\boldsymbol{b}^2} \tag{2.1}$$

Here, β represents the FWHM of the GaN peak, and $\boldsymbol{b}$ represents the Burgers vector of the associated dislocation. Note that D_B is directly proportional to the FWHM of the associated GaN peak, and therefore an improvement in the GaN crystal quality is indicated by a narrowing of the FWHM. Simultaneously, the improvement in quality of the GaN layer is also accompanied by an increase in the mean crystallite size (τ) due to the reduction in D_B. The mean crystallite size and FWHM of the GaN diffraction pattern can be related by the Scherrer equation:

$$\tau = \frac{K\lambda}{\beta \sin\theta} \tag{2.2}$$

Here, K is a dimensionless shape factor, λ is the wavelength of the x-ray, β represents the FWHM of the GaN peak and θ is the Bragg's angle for the GaN diffraction.

2.3.1 Mitigation of crystal properties of polycrystalline GaN by thermal annealing

RF-sputtering and e-beam evaporator both provide simple yet effective way to deposit GaN layer. Even so, these techniques are rarely explored and manipulated, especially in GaN research, i. e. in [26-28]. As been mentioned earlier, most of the systems only operate at room temperature, hence tends to produce poor properties of the GaN layer.

To overcome this problem, we propose post-annealing treatment to the GaN layer as an attempt to improve the crystal structure of the layer via solid phase recrystallization after the deposition by RF-sputtering and e-beam evaporator. Through solid phase recrystallization, TDs in the grains boundaries can be eliminated, and therefore reducing the FWHM through recrystallization during the annealing. Such approach has been reported to improve the crystal quality of nitrides as reported by [58]. It should be concerned that the annealing conditions, including

temperature and gas ambient play significant role to improve the properties of the GaN layer. For example, in the report [28], the maximum annealing temperature was as low as 600 ^{o}C. It is suspected that this temperature is not sufficient to promote better surface morphology.

Conducting annealing at low temperature would not promote sufficient improvement [28] recrystallization due to limited supply of thermal energy. On the other hand, high temperature would result in severe thermal decomposition of the GaN layer [58]. S. Yeonwoo *et.* al. [36] suggested that the best temperature to improve structural properties of polycrystalline GaN layer is ~950 ^{o}C.

Generally, annealing in nitrogen (N_2) environment only serves to improve the structural and surface morphology quality of a GaN layer by recrystallization [58]. However, it does not exhibit the same effect on the optical properties of the GaN layer [59]. Alternatively, annealing in ammonia (NH_3) is beneficial for the GaN layer, which normally suffers high N-deficiency on the surface. It is imperative to acknowledge that NH_3 dissociates into nitrogen (N) and hydrogen (H) upon heating [60].

$$2\,NH_3 \underset{\Delta}{\rightarrow} N_2 + 3H_2 \tag{2.3}$$

The active N atoms will be used to reduce the N-deficiency on the surface of the GaN layer while recrystallizing the GaN layer to form into a better structure. However, without any catalyst, only a certain percentage of NH_3 gas will undergo the dissociation in a given volume. The non-dissociated NH_3 gas would later cause surface etching on the GaN layer [61]. Meanwhile, the H byproduct is known to passivate the GaN layers [59]. The dissociation rate for NH_3 gas was reported to be

~16% at a temperature of 650 ^{o}C, and exhibits an increasing trend as the temperature increases [60].

Previous report on annealing GaN layers in NH_3 involves an extended annealing time, typically in the range of few hours [24, 25]. This is due to the gas flow rate used, which was in the range of 500 standard cubic centimeters per minute (SCCM). The low gas flow rate will limit the rate, where the active N atoms incorporate into the GaN lattice sites, and thus a longer annealing time is needed to improve the quality of the GaN layer. In contrast, this work proposed to use a higher flow rate in the range of few standard liter per minute (SLM) to increase the rate, where the N atoms incorporate into the GaN lattice sites, hence reducing the annealing time required to improve the GaN layer.

The NH_3 gas flow rate with the most effective incorporation of active N atoms into the lattice site of GaN layer is one of the element of interest in this work. Published works, that relates to the gas flow rate and incorporation of active N atoms are vague. However, in order to determine a suitable NH_3 flow rate, the following basis is considered: A flow rate that is too low causes the non-dissociated NH_3 gas to stay stagnant. This causes 'clouding' of NH_3 gas on the surface, which reduces the effectiveness of the N atoms to incorporate into the GaN lattice on the surface. On the other hand, a high gas flow rate regime will cause the active N atoms to pass over the sample surface quickly towards the exhaust outlet, which also leads to similar results, as in the case of the low gas flow rate. This means that the N-deficiency will not be minimized in both cases.

2.3.2 Deposition of AlN buffer layer as a strategy to improve polycrystalline GaN properties

Due to the heteroepitaxy nature, the GaN layer grown on foreign substrate is typically under stress [62], hence acting as physical strain in the form of bowing [63]. Inserting an AlN buffer layer has been a common way to reduce this stress [29] and subsequently to improve the quality of the overlying GaN layer [30]. In this work, an attention is given to optimize the buffer layer thickness. If the AlN buffer layer were too thin, it will result in an insufficient improvement of the GaN layer [64], while if it is too thick, poor electrical properties will be expected. Therefore, a series of AlN buffer layer with different thickness is worth to be included in this work.

This work proposed to use solid Al source before reacting with a N_2 source to form AlN buffer layer for polycrystalline GaN. Due to the ability of the sputtering system to generate N_2 plasma, AlN layers will be deposited by sputtering, as opposed to e-beam evaporator. In this work, the maximum thickness of AlN buffer layer deposited by sputtering should not exceed a critical thickness of ~170 nm, as a thicker layer would have lower structural quality [58], while degrading electrical property of the device [6].

2.4 Principle of metal-semiconductor-metal (MSM) photodetector

Photodetector is a device, which converts light into electrical signal. Among the commonly used structures such as a p-n junction [65], semiconductor-insulator-semiconductor (p-i-n) [66], and metal-insulator-semiconductor (MIS) [67]. Nonetheless, this work proposes to develop photodetector based on metal-semiconductor-metal (MSM) structure using polycrystalline GaN material. This is due to its simple operation, requires inexpensive fabrication and process, and its